

Polarization-Sensitive and Broadband Photodetection Based on a Mixed-Dimensionality TiS_3/Si p–n Junction

Yue Niu, Riccardo Frisenda,* Eduardo Flores, Jose R. Ares, Weicheng Jiao, David Perez de Lara, Carlos Sánchez, Rongguo Wang, Isabel J. Ferrer,* and Andres Castellanos-Gomez*

The capability to detect the polarization state of light is crucial in many day-life applications and scientific disciplines. Novel anisotropic 2D materials such as TiS_3 combine polarization sensitivity, given by the in-plane optical anisotropy, with excellent electrical properties. Here, the fabrication of a monolithic polarization-sensitive broadband photodetector based on a mixed-dimensionality TiS_3/Si p–n junction is demonstrated. The fabricated devices show broadband responsivity up to 1050 nm, a strong sensitivity to linearly polarized illumination with difference between the two orthogonal polarization states up to 350%, and a good detectivity and fast response time. The discussed devices can be used as building blocks to fabricate more complex polarization-sensitive systems such as polarimeters.

polarization-sensitive photodetectors and polarimeters.^[6] Up to now, however, most of the reported works on photodetectors based on 2D semiconductors are focused on transition metal dichalcogenides or other chalcogenides with marked in-plane isotropic properties and thus the built-up photodetectors are insensitive to polarized light.^[3a,7] The amount of works exploring the use of dichroic 2D semiconductors is still scarce and they are mostly limited to devices with low detectivity values or with a limited cut-off wavelength.^[8] Recently, Island et al. have fabricated photodetectors using TiS_3 ,^[7c] a member of the trichalcogenide family that presents remarkable

quasi-1D electrical and optical properties with an anisotropy larger than the one of black phosphorus.^[9] However, this strong in-plane anisotropy has not been exploited yet to fabricate polarization-sensitive photodetectors.

Here, we demonstrate the fabrication of monolithic polarization-sensitive photodetectors based on TiS_3 . The devices are built up by staking a TiS_3 ribbon onto p-type silicon, thus forming a p–n junction based photodiode geometry which allows one to operate the device either in photovoltaic (PV) mode, without applying any external bias, or in photoconductive (PC) mode, with a positive or negative bias applied to the device. In PV mode upon illumination, the built-in electric field present at the interface between TiS_3 and Si separates the photogenerated charge carriers yielding to photocurrent even under unbiased condition. The fabricated devices show broadband photoresponse from 405 to 1050 nm and a strong dependence of their photoresponse on the polarization

1. Introduction

Polarization-sensitive photodetectors, which are optoelectronic devices sensitive to the polarization of the incoming light, have a strong impact in many different branches of science and technology like astronomy,^[1] quality assessment in food and mechanical industry,^[2] and ellipsometry.^[3] Natural evolution endowed certain animals and insects with eyes equipped with monolithic polarization-sensitive photodetectors. These specialized light detectors facilitate the identification of their preys or allow them to navigate recognizing the polarization patterns of the sky.^[4] Interestingly, similar navigation techniques based on the detection of polarization patterns of the sky have been probably used by ancient civilizations during human history.^[5] The recent isolation of strongly dichroic 2D semiconductors holds a great promise for the fabrication of monolithic


Y. Niu, Prof. W. Jiao, Prof. R. Wang
Science and Technology on Advanced Composites in Special
Environments Laboratory
Harbin Institute of Technology
150080 Harbin, P. R. China

Y. Niu, Dr. R. Frisenda, Dr. D. Perez de Lara
Madrid Institute for Advanced Studies (IMDEA Nanociencia)
Ciudad Universitaria de Cantoblanco
Calle Faraday 9, 28049 Madrid, Spain
E-mail: riccardo.frisenda@imdea.org

Dr. E. Flores, Dr. J. R. Ares, Prof. C. Sánchez, Prof. I. J. Ferrer
Materials of Interest in Renewable Energies Group (MIRE Group)
Dpto. de Física de Materiales
Universidad Autónoma de Madrid (UAM)
Campus de Cantoblanco, E-28049 Madrid, Spain
E-mail: isabel.j.ferrer@uam.es

Prof. C. Sánchez, Prof. I. J. Ferrer
Instituto Nicolás Cabrera
Universidad Autónoma de Madrid (UAM)
Campus de Cantoblanco, E-28049 Madrid, Spain

Dr. A. Castellanos-Gomez
Materials Science Factory
Instituto de Ciencia de Materiales de Madrid (ICMM-CSIC)
Madrid E-28049, Spain
E-mail: andres.castellanos@csic.es

 The ORCID identification number(s) for the author(s) of this article can be found under <https://doi.org/10.1002/adom.201800351>.

DOI: 10.1002/adom.201800351

direction of the illumination. The photocurrent generated for light polarized along the b -axis direction of the TiS_3 lattice is up to 350% larger than that polarized along the a -axis direction. These devices can be used as building blocks to fabricate more complex thin polarization-sensitive systems such as polarimeters.

2. Results and Discussion

Figure 1a,b shows optical images of synthesized TiS_3 microcrystals with a characteristic ribbon-like shape.^[10] **Figure 1c** shows a representation of the crystal structure of TiS_3 , a monoclinic ZrSe_3 -type lattice with two lattice vectors per unit cell. The atoms are separated in layers that are held together by van der Waals interactions and each layer is composed of parallel covalently bonded chains. Each Ti atom is bonded to six S atoms belonging to the same chain and two additional S atoms in the neighbor chains.^[9a,b,11] The parallel chains are responsible for the quasi-1D nature of the material which leads to an anisotropy in the electrical conductivity and optical properties between the in-plane a - and b -axes.

Figure 1d shows various microtransmittance spectra acquired on a TiS_3 ribbon while varying the relative orientation between the linearly polarized incident light and the b -axis of the TiS_3 ribbon.^[12] One can clearly see the gradual evolution of the transmittance spectra using light with polarization angles ranging from aligned along the a direction to the b direction. The transmittance along the b -axis is quite low (52% at 2.32 eV) and the ribbon appears darker due to the larger absorption. In contrast, the transmittance along the a -axis reaches 71% at 2.32 eV and the ribbon becomes much more transparent (see a movie of the polarization-dependent transmittance in the Supporting Information). **Figure 1e** shows a polar plot of the transmittance at different wavelengths as a function of the orientation between the linearly polarized light and the b -axis. The minimum (maximum) of transmittance occurs for light polarized in the direction the b -axis (a -axis). This twofold polarization-angle-dependent absorption feature can be explained by the strong difference in the electrical conductance about the b -axis (highly conductive) and the a -axis (poorly conductive) observed in TiS_3 , analogously to what happens in wire grid polarizers.^[9] In fact, recent ab initio calculations based on the Bethe–Salpeter equation show that the transmittance and the absorption coefficient of TiS_3 show a marked twofold polarization angle dependence.^[9b,c] Moreover, in order to prove that this optical spectra anisotropy stems from the anisotropic crystal structure of the TiS_3 and not from a geometrical effect (e.g., nanowire wave guiding) we show in the Supporting Information a similar transmission spectra measurement on a TiS_3 sample with very low aspect ratio displaying very similar features.

To fabricate the TiS_3 -based photodetectors, we employ mechanical exfoliation combined with deterministic transfer of ultrathin TiS_3 ribbons.^[13] **Figure 2** summarizes the steps carried out to fabricate the devices. The commercial substrate is based on prepatterned Cr/Au electrodes evaporated on SiO_2/Si (Ossilla). We mask the electrodes using a piece of kapton tape and we etch away the unmasked SiO_2 using a glass etchant paste (ArmourEtch) that effectively removes the SiO_2 without damaging the Si bottom layer. Note that this is a very convenient way to etch the SiO_2 without employing extremely dangerous

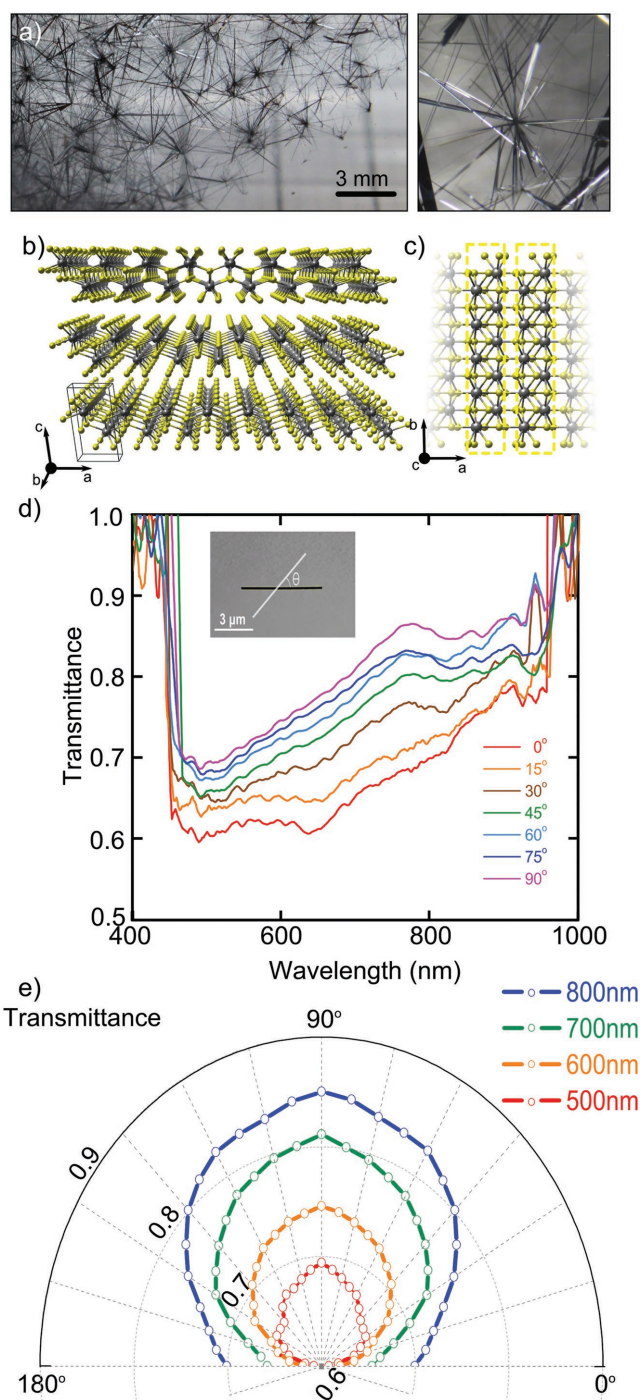


Figure 1. a) Photograph of TiS_3 and magnified photograph of TiS_3 ribbons. b) Artistic representation of the crystal structure of TiS_3 . The gray spheres represent the Ti atoms and the yellow spheres represent the S atoms. The unit cell is indicated by solid black lines. c) Artistic representation of the TiS_3 unit cell. d) Differential transmittance spectra of a TiS_3 nanoribbon deposited onto PDMS measured as a function of the polarization angle of the transmitted radiation. Inset: Photograph of a TiS_3 ribbon (the white solid line defines the polarization angle). e) Polar plot of the transmittance of a TiS_3 nanoribbon at different wavelengths.

buffered hydrofluoric (HF) acid etching recipes. Finally, the device is completed by transferring a TiS_3 ribbon by means of

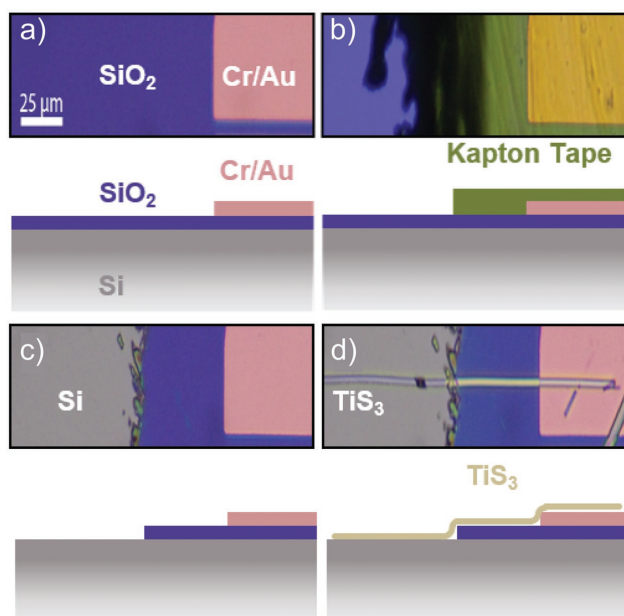


Figure 2. Schematic diagram of preparation process of TiS_3/Si p–n junction. a) Prepatterned Cr/Au electrode on SiO_2/Si Substrate. b) Covering electrode with kapton tape. c) Etching the SiO_2 from Si Substrate. d) Preparing the p–n junction by transferring a TiS_3 nanoribbon onto the partially exposed Si substrate.

an all dry deterministic transfer method bridging one of the Au/Cr electrodes to the exposed Si surface.^[14]

The optoelectronic performances of the fabricated TiS_3 devices are characterized in dark and upon illumination using a home-made scanning photocurrent system.^[15] **Figure 3a** shows the IV characteristics of a TiS_3 device in dark and upon illumination (with 660 nm of wavelength) with increasingly optical power. In the dark state, the device shows a marked rectifying IV due to the p–n junction formed at the interface between the TiS_3 (n-type semiconductor) and the silicon (p-type, boron doped with a resistivity of 0.0005–0.001 $\Omega \cdot \text{cm}$). The rectifying IV can be modeled by the Shockley diode equation (see the Supporting Information) as shown in the inset of **Figure 3a**. The fit reproduces well the experimental IV when considering a series resistance of 270 k Ω (the fit parameters are listed in Table S1 in the Supporting Information). This series resistance takes into account the contributions of the TiS_3 internal resistance and the contact resistance between TiS_3 and Au.

Under external illumination, we observe an increase in the current. The reverse current (current at negative bias) increases monotonically upon increasing the incident power. **Figure 3b** shows the details of the IV s at low bias voltage. At zero bias voltage, the built-in electric field at the interface between the TiS_3 and the silicon separates the photogenerated electron–hole pairs giving rise to the so-called short-circuit current (I_{sc}), a clear signature of the PV photocurrent generation mechanism. The open-circuit voltage (V_{oc}) is also a signature of the built-in electric field. Both I_{sc} and V_{oc} increase as the incident optical power increases (see the Supporting Information for more details).

Figure 3c shows the photoresponsivity of the device measured at -0.5 V by employing illumination sources with

different wavelengths. The photoresponsivity, R , is a measure of the electrical response to light and is defined as

$$R = I_{\text{ph}} / P_{\text{in}} \quad (1)$$

where P_{in} is the incident optical power. The shape of the responsivity spectrum follows closely that of the unpolarized microabsorbance spectrum of the TiS_3 ribbon, calculated from the transmittance according to the formula

$$A = -\log(T) \quad (2)$$

suggesting that the photoresponse is dominated by the interaction of light with the TiS_3 itself. These results are in good agreement with the previously reported experimental values obtained from photocurrent response and optical absorbance measurements of TiS_3 .^[16] Besides, to evaluate the performance of TiS_3/Si as a photodetector, we calculate the inferred detectivity (D^*), which represents the ability to detect weak optical signals. Assuming the noise to be limited by shot noise, D^* is calculated from the measured responsivity and the dark current^[17] according to

$$D^* = R \cdot A_d^{1/2} / (2eI_d)^{1/2} \quad (3)$$

where A_d is effective area of the device, e is the electron charge, and I_d is the dark current. The calculated D^* value reaches 2.5×10^8 Jones at bias voltage of 0 V and 2.65×10^9 Jones at -0.5 V for the device shown in the main text (other devices reach up to 2.65×10^9 Jones and 1.3×10^{10} , respectively). The summarized photonic parameters (R , D^* , response time) and comparison with reported anisotropic photodetectors are shown in **Table 1**. Consequently, the superior efficiency of the detectivity of our TiS_3/Si devices is comparable to black phosphorus/ WSe_2 heterojunction^[17b] and one or two magnitudes larger than other reported anisotropic photodetectors,^[8b,c] which we attribute to the strong intrinsic responsivity of TiS_3 together with the photodiode device architecture that minimizes the dark current.^[7c] However, Tan et al. reported a photodetector based on GeS shows a rather high detectivity but operating at high temperature.^[17a] Also, the devices like GeS and ReS_2 have slower response times and limited cut-off wavelength of 800 nm.^[8c,17a]

The electrical and PV properties manifested by the TiS_3 –Si device can be explained by the band diagram of the two materials schematically depicted in **Figure 3d**. The isolated materials (left panel) are semiconductors with bandgap energies of 1.10 and 1.12 eV, respectively, for TiS_3 and Si. The difference in the position of the Fermi levels of the isolated materials induces a charge transfer that creates a built-in electric field, when the two materials are brought in contact. This phenomenon is shown in the band diagram by the bending of both the conduction and the valence band at the interface between the two materials (see the right panel of **Figure 3d**). The rectifying IV s and the PV effect observed in our devices are consistent with such a band diagram.

Taking advantage of the high-speed optical communication and high responsivity of our devices, we demonstrated a single-pixel camera^[18] based on an ultrathin TiS_3/Si photodetector. A scheme of the single-pixel camera setup integrated with our TiS_3/Si devices is shown in **Figure 4a**.^[12] Briefly, the target

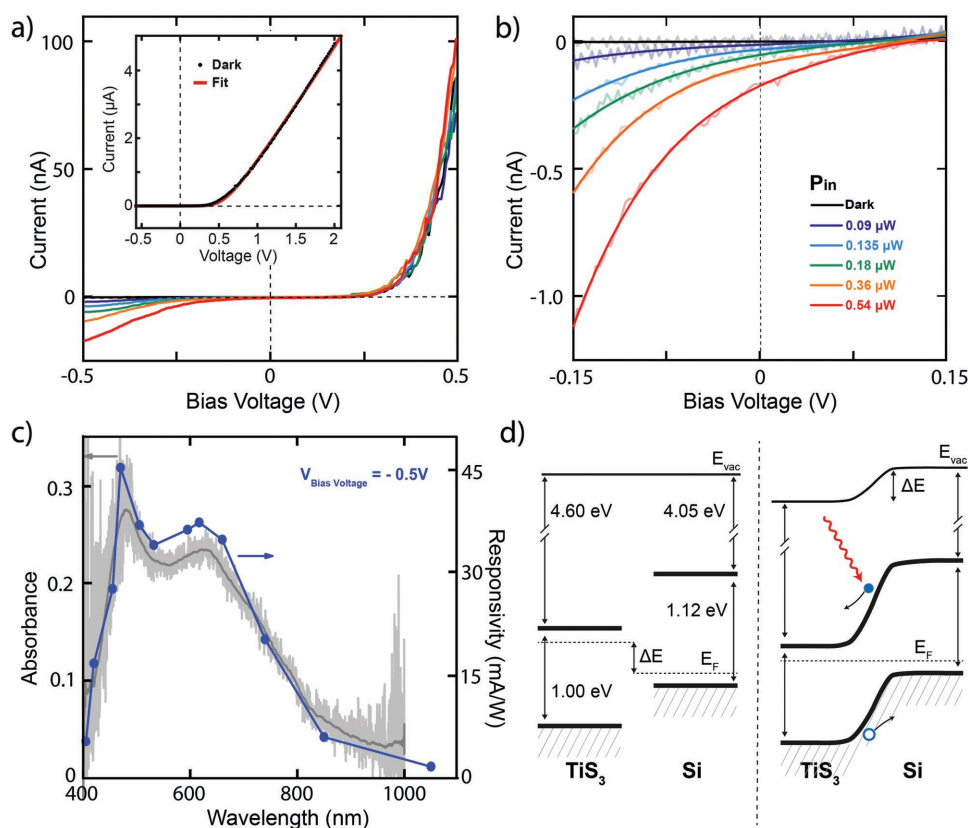


Figure 3. a) Current versus bias voltage characteristics of the device in dark and upon illumination with increasingly optical power. Inset: fit of the current versus bias voltage characteristic recorded in dark to the Shockley diode equation. b) Zoomed-in plot of current versus bias voltage characteristics of the device. c) Responsivities (blue line) for different illumination wavelengths with an incident optical power of $0.54 \mu\text{W}$ and a bias voltage of -0.5 V . The responsivities are compared with the microabsorbance spectrum (gray line) of TiS_3 on PDMS. d) Band diagram of isolated TiS_3 and Si (left) and of the heterojunction between the two materials (right).

to image is mounted on a motorized XY stage, which can be controlled by the computer. The target is illuminated from the bottom by a white light source. An optical fiber, positioned on top of the target image, acts as a pinhole, thus only collecting the light coming from a small region of the target. The free end of the fiber is connected to a cannula to irradiate directly the TiS_3/Si photodetector reversely biased. Whilst illuminating the sample, the device electrical properties are measured with a Keithley 2450 source meter unit as a function of the spot position. From the spatial map of the photocurrent, we can reconstruct a photograph of the target where optically dark areas correspond to low photocurrent signals and bright areas to large photocurrent. The data acquisition and motion control are managed through a home-made routine written in Matlab. To test the effectiveness of the camera, a “Smiley Face” was used as a target and the recovered image with a resolution of 64×64 pixels is shown in Figure 4b. In spite of the simplicity of the single-pixel camera setup, it provides a testbed to explore the performance of photodetectors based on nanomaterials in real-life applications.

After testing the optoelectronic properties of TiS_3/Si junctions for unpolarized light, we now discuss the performances of these devices for polarized light detection. Figure 5a,b shows the IV curves of the device upon illumination with linearly polarized light at 660 nm of wavelength and optical

power of $0.54 \mu\text{W}$. The polarization of the illumination has been varied from linearly polarized along the b -axis (labeled as 0° in the figure) to linearly polarized along the a -axis (labeled as 90° in the figure). From the IVs, it is clear that the photoresponse of the device depends on the relative orientation between the linearly polarized illumination and the crystal orientation of the TiS_3 ribbon, as expected from the strong linear dichroism observed in the absorbance of the material. The inset shows the relationship between the photodetector responsivity (extracted at 660 nm) and the relative angle between the incident linearly polarized light with respect to the b -axis. Figure 5c,d shows two polar plots with the polarization orientation dependence of the photocurrent extracted at -2 V (mainly due to PC photocurrent generation) and short-circuit current at 0 V (due to PV effect). The anisotropy in the photocurrent response stems from the anisotropic crystal structure of TiS_3 . In fact, as shown above, the absorption of photons polarized along the b -axis is stronger than that for photons polarized along the a -axis. The maximum photocurrent, corresponding to a photoresponsivity R of $\approx 35 \text{ mA W}^{-1}$, is reached for incident light polarized along b -axis. The minimum response is $\approx 19 \text{ mA W}^{-1}$ with incident light polarized along a -axis. As shown in Table 1, this polarization photosensitivity values are comparable with those of recently reported black phosphorus based polarized photodetectors.^[8b,17b] These

Table 1. Performance comparison of our TiS₃/Si devices with reported anisotropic photodetectors.

Device	Measurement	Self-powered	Cut-off wavelength [nm]	R ^{a)} [mA W ⁻¹]	D ^{a,b)} [cm Hz ^{1/2} W ⁻¹]	Response time [ms]	Anisotropy ratio	Ref.
TiS ₃ /Si heterojunction	660 nm V = -0.5 V/0 V	Yes	>1050	34.8/0.33	1.04 × 10 ¹⁰ /2.5 × 10 ⁸	<20	0.29/0.44	This work main text
				18.3/0.31	1.3 × 10 ¹⁰ /2.9 × 10 ⁸	<20	0.21/0.49	Sample 2
				8.5/2.63	3.36 × 10 ⁹ /1.9 × 10 ⁹	<20	0.26/0.38	Sample 3
				18.9/3	6.63 × 10 ⁹ /2.65 × 10 ⁹	<20	0.24/0.64	Sample 4
Black phosphorus	1200 nm, V = 0.1 V	No	3750	0.35	4.13 × 10 ⁷ (^{c)})	0.04	0.56	[8b]
Black phosphorus	785 nm, V = -10 V	No	N/A	N/A	N/A	N/A	0.3	[8d]
ReS ₂	405 nm, V = 1 V	No	800	1.2 × 10 ⁶	5 × 10 ¹¹ (^{c)})	98	0.5(^{c)})	[8e]
ReSe ₂	633 nm, V _{ds} = 0.5 V	No	1000	1.5	1.19 × 10 ⁸ (^{c)})	2	0.33(^{c)})	[8c]
GeS	500 nm V _{ds} = 4 V, 373 K	No	800	2.4 × 10 ⁶	1.5 × 10 ¹⁴	N/A	>0.9(^{c)})	[17a]
InP	N/A	No	N/A	3 × 10 ⁶	N/A	N/A	0.96	[19a]
SWNT	970 nm V _{ds} = 1 V V _g = -1.5 V	No	980	N/A	N/A	N/A	0.22(^{c)})	[19b]
Black phosphorus/MoS ₂	532 nm, V = 2 V	Yes	>1550	170	4.9 × 10 ⁸ (^{c)})	N/A	0.43(^{c)})	[8a]
Black phosphorus/WSe ₂	1550 nm, V = 0.5 V	No	>1550	5 × 10 ²	10 ¹⁰	0.8	0.71(^{c)})	[17b]

N/A: not applicable; ^{a)}Responsivity of the device; ^{b)}Detectivity of the device with the conditions specified in the column "Measurement"; ^{c)}The value calculated from the data extracted from the reference but not stated directly in the cited article. Note that in some columns, we display two values for our devices, they correspond to the values obtained under V = -0.5 V and V = 0 V, respectively.

figure of merits found for the TiS₃/Si photodetector device are comparable with those of available devices. Specifically, R is very close to the responsivity of commercial Si-based photodiodes (Thorlabs S120C, R = 55 mA W⁻¹). Moreover, the sensitivity of TiS₃ to the polarization of the incident light allows to fabricate more compact polarization-sensitive photodetectors compared with conventional Si photodetectors where there is a need of using an external polarizer element. The maximum anisotropy ratio of the photocurrent (measured at -0.5 V) and short-circuit current

$$\bar{\sigma} = (I_{\max} - I_{\min}) / (I_{\max} + I_{\min}) \quad (4)$$

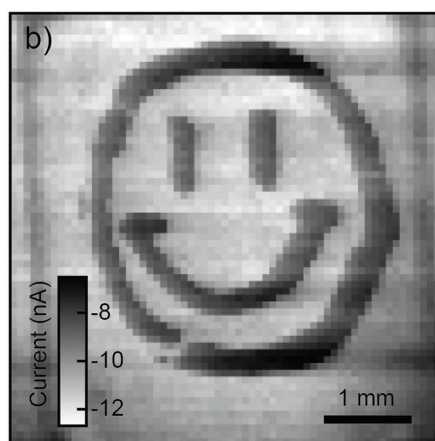
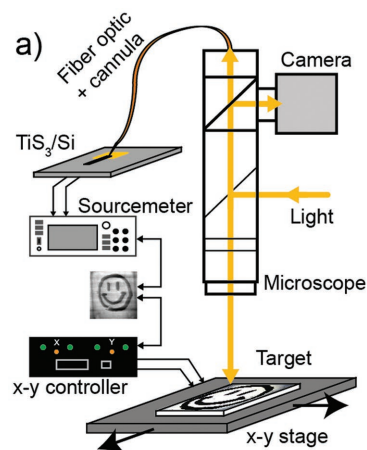


Figure 4. a) Schematic of the experimental system for single-pixel camera. b) The recovered image by the single-pixel camera of the TiS₃/Si photodetector with 64 × 64 pixels at -1 V.

of the device is 0.29 and 0.64, respectively, which is comparable with the angular-dependent photocurrent in other phototransistors (from 0.3 to 0.96).^[8,17,19] However, those polarization-sensitive photodetectors typically require an external bias as the driving force to prevent the recombination of photogenerated electron-hole pairs and their dark current is larger (thus typically yielding to lower detectivity values). We address the reader to the Supporting Information to see the full characterization of another three TiS₃/Si photodetector devices.

Figure 6 shows a spatially resolved characterization of the device photoresponse. The incident light at 660 nm with the power of 0.54 μW was applied (the motor step size is 3 μm). **Figure 6a** shows an optical image of the studied device region. **Figure 6b** shows four photocurrent maps acquired rotating the relative orientation between the linearly polarized light and the TiS₃b-axis. The different regions of the device, outlined in the photocurrent maps, are determined from reflectivity maps acquired simultaneously (see the Supporting Information). Interestingly, from the photocurrent maps one can clearly observe how the photocurrent is only generated at the TiS₃/Si junction, which is because of the charge separation, happens right at the heterojunction region.

3. Conclusion

In summary, we presented a self-powered polarization-sensitive photodetector based on a

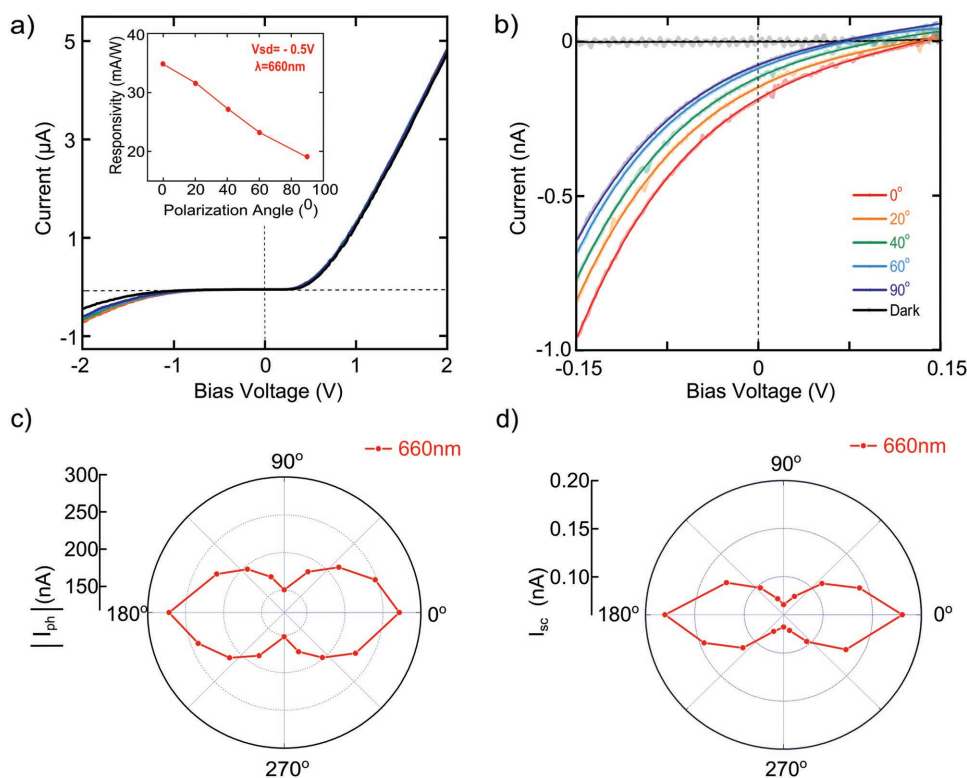


Figure 5. a) Current versus bias voltage characteristics of the TiS_3/Si device upon illumination with increasing polarization angle. b) A zoomed-in plot around zero bias to show the PV effect upon illumination. c) Polar plot of the absolute value of photocurrent at a bias voltage of -2 V . d) Polar plot of the absolute value of the short-circuit current.

TiS_3/Si p–n junction. The heterostructure device demonstrates a broadband photodetecting range (from 405 to 1050 nm) with high photoresponsivity ($\approx 35\text{ mA W}^{-1}$), but also shows a high sensitivity to polarized infrared illumination photodetection. The polarized

contrast between b - and a -axis direction of the TiS_3 lattice is up to 350%. Our novel heterojunction structure offers an ideal candidate for future 2D optoelectronic devices with unique anisotropic nature.

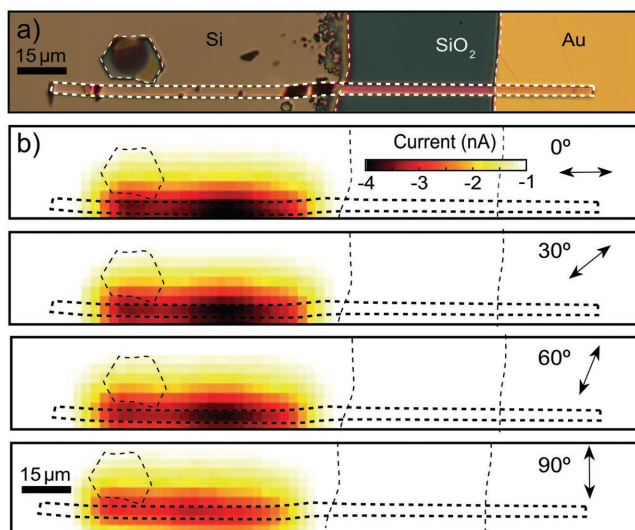


Figure 6. a) Optical image of the p–n heterojunction used for photocurrent mapping. b) Scanning photocurrent map of the p–n heterojunction at different polarization angles. The dashed lines outline the important spatial features of the device.

4. Experimental Section

TiS_3 Preparation: The TiS_3 microcrystals were synthesized by sulfuration of titanium powder which was vacuum sealed in an ampule with sulfur powder (>75% atomic sulfur) and heated to 500°C . After 20 h of growth, the ampule was cooled down to ambient conditions.^[10]

Characterizations: The atomic force microscopy of the devices was performed with a commercial head and software from Nanotec. The as-grown TiS_3/Si heterostructure devices were annealed at 200°C for 2 h in vacuum to improve the contact for the devices. The optical properties of the nanosheets had been studied with a home-built microreflectance/transmittance spectroscopy setup, described in detail in ref. [12]. The transmittance (Figure 1) and absorbance (Figure 3) data had been obtained through differential measurements. Two spectra were acquired: one on the bare substrate (I_0) and the other on the TiS_3 sample (I). The transmittance (T) was then calculated as $T = I/I_0$ and the absorbance (A) was $A = -\log_{10}T$. Therefore, the absorption of the PDMS substrate was accounted for in the calculation of these magnitudes. These devices were characterized by a semiconductor analyzer Keithley 2450 and a home-built probe station.

Supporting Information

Supporting Information is available from the Wiley Online Library or from the author.

Acknowledgements

The authors acknowledge funding from the EU Graphene Flagship (Grant Graphene Core2 785219) and from the European Research Council (ERC) under the European Union's Horizon 2020 research and innovation program (grant agreement no. 755655, ERC-StG 2017 project 2D-TOPSENSE). R.F. acknowledges support from the Netherlands Organisation for Scientific Research (NWO) through the research program Rubicon with project number 680-50-1515. D.P.d.L. acknowledges support from the MINECO (program FIS2015-67367-C2-1-P). Y.N. acknowledges the grant from the China Scholarship Council (File No. 201506120102). W.C.J. acknowledges the Program for the Top Young and Middle-aged Innovative Talents of Harbin Institute of Technology. MIRE group acknowledges financial support from MINECO-FEDER (MAT2015-65203-R).

Conflict of Interest

The authors declare no conflict of interest.

Keywords

optoelectronic devices, photodetectors, p–n junctions, polarimeters, titanium trisulfide, trichalcogenides

Received: March 17, 2018

Revised: June 21, 2018

Published online: July 25, 2018

- [1] a) B. Cairns, E. E. Russell, J. D. LaVeigne, P. M. Tennant, *Proc. SPIE* **2013**, 5158, 33; b) M. D. Niemack, P. Ade, J. Aguirre, F. Barrientos, J. Beall, J. Bond, J. Britton, H. Cho, S. Das, M. Devlin, *Proc. SPIE* **2010**, 7741, 77411S.
- [2] N. A. Hagen, D. S. Sabatke, J. F. Scholl, P. A. Jansson, W. W. Chen, E. L. Dereniak, D. T. Sass, *Polarization Sci. Remote Sensing* **2003**, 5158, 45.
- [3] a) R. M. Azzam, N. M. Bashara, *Ellipsometry and Polarized Light*, North-Holland, Amsterdam, The Netherlands **1987**; b) I. Mandel, J. N. Gollub, I. Bendoy, D. T. Crouse, *IEEE Sens. J.* **2013**, 13, 618.
- [4] a) G. Horváth, M. Blahó, G. Kriska, R. Hegedüs, B. Geric, R. Farkas, S. Åkesson, *Proc. R. Soc. London, Ser. B* **2010**, 277, 1643; b) G. Horváth, P. Malik, G. Kriska, H. Wildermuth, *Freshwater Biol.* **2007**, 52, 1700; c) N. Shashar, R. T. Hanlon, A. M. Petz, *Nature* **1998**, 393, 222.
- [5] G. Horváth, A. Barta, I. Pomozi, B. Suhai, R. Hegedüs, S. Åkesson, B. Meyer-Rochow, R. Wehner, *Proc. R. Soc. London, Ser. B* **2011**, 366, 772.
- [6] a) S. Z. Butler, S. M. Hollen, L. Cao, Y. Cui, J. A. Gupta, H. R. Gutiérrez, T. F. Heinz, S. S. Hong, J. Huang, A. F. Ismach, *ACS Nano* **2013**, 7, 2898; b) A. Castellanos-Gomez, *Nat. Photonics* **2016**, 10, 202; c) D. Jariwala, T. J. Marks, M. C. Hersam, *Nat. Mater.* **2017**, 16, 170; d) F. Koppens, T. Mueller, P. Avouris, A. Ferrari, M. Vitiello, M. Polini, *Nat. Nanotechnol.* **2014**, 9, 780; e) Q. H. Wang, K. Kalantar-Zadeh, A. Kis, J. N. Coleman, M. S. Strano, *Nat. Nanotechnol.* **2012**, 7, 699; f) F. Xia, H. Wang, D. Xiao, M. Dubey, A. Ramasubramaniam, *Nat. Photonics* **2014**, 8, 899.
- [7] a) M. Buscema, J. O. Island, D. J. Groenendijk, S. I. Blanter, G. A. Steele, H. S. van der Zant, A. Castellanos-Gomez, *Chem. Soc. Rev.* **2015**, 44, 3691; b) J. O. Island, S. I. Blanter, M. Buscema, H. S. van der Zant, A. Castellanos-Gomez, *Nano Lett.* **2015**, 15, 7853; c) J. O. Island, M. Buscema, M. Barawi, J. M. Clamagirand, J. R. Ares, C. Sánchez, I. J. Ferrer, G. A. Steele, H. S. van der Zant, A. Castellanos-Gomez, *Adv. Opt. Mater.* **2014**, 2, 641; d) J. O. Island, A. J. Molina-Mendoza, M. Barawi, R. Biele, E. Flores, J. M. Clamagirand, J. R. Ares, C. Sánchez, H. S. van der Zant, R. D'Agosta, I. J. Ferrer, A. Castellanos-Gomez, *2D Mater.* **2017**, 4, 022003; e) O. Lopez-Sanchez, D. Dumcenco, E. Charbon, A. Kis, *arXiv Preprints* **2014**, arXiv:1411.3232; f) O. Lopez-Sanchez, D. Lembke, M. Kayci, A. Radenovic, A. Kis, *Nat. Nanotechnol.* **2013**, 8, 497.
- [8] a) T. Hong, B. Chamlagain, T. Wang, H.-J. Chuang, Z. Zhou, Y.-Q. Xu, *Nanoscale* **2015**, 7, 18537; b) H. Yuan, X. Liu, F. Afshinmanesh, W. Li, G. Xu, J. Sun, B. Lian, A. G. Curto, G. Ye, Y. Hikita, *Nat. Nanotechnol.* **2015**, 10, 707; c) E. Zhang, P. Wang, Z. Li, H. Wang, C. Song, C. Huang, Z.-G. Chen, L. Yang, K. Zhang, S. Lu, *ACS Nano* **2016**, 10, 8067; d) T. Hong, B. Chamlagain, W. Lin, H.-J. Chuang, M. Pan, Z. Zhou, Y.-Q. Xu, *Nanoscale* **2014**, 6, 8978; e) F. Liu, S. Zheng, X. He, A. Chaturvedi, J. He, W. L. Chow, T. R. Mion, X. Wang, J. Zhou, Q. Fu, *Adv. Funct. Mater.* **2016**, 26, 1169.
- [9] a) J. O. Island, M. Barawi, R. Biele, A. Almázan, J. M. Clamagirand, J. R. Ares, C. Sánchez, H. S. J. van der Zant, J. V. Álvarez, R. D'Agosta, I. J. Ferrer, A. Castellanos-Gomez, *Adv. Mater.* **2015**, 27, 2595; b) J. O. Island, R. Biele, M. Barawi, J. M. Clamagirand, J. R. Ares, C. Sánchez, H. S. Van Der Zant, I. J. Ferrer, R. D'Agosta, A. Castellanos-Gomez, *Sci. Rep.* **2016**, 6, 22214; c) N. Papadopoulos, R. Frisenda, R. Biele, E. Flores, J. R. Ares, C. Sánchez, H. S. J. van der Zant, I. J. Ferrer, R. D'Agosta, A. Castellanos-Gomez, *Nanoscale* **2018**, 10, 12424.
- [10] a) A. J. Molina-Mendoza, J. O. Island, W. S. Paz, J. M. Clamagirand, J. R. Ares, E. Flores, F. Leardini, C. Sánchez, N. Agrait, G. Rubio-Bollinger, H. S. J. van der Zant, I. J. Ferrer, J. J. Palacios, A. Castellanos-Gomez, *Adv. Funct. Mater.* **2017**, 27, 1605647; b) I. J. Ferrer, M. Maciá, V. Carcelén, J. R. Ares, C. Sánchez, *Energy Proc.* **2012**, 22, 48.
- [11] J. Silva-Guillén, E. Canadell, P. Ordejón, F. Guinea, R. Roldán, *2D Mater.* **2017**, 4, 025085.
- [12] R. Frisenda, Y. Niu, P. Gant, A. J. Molina-Mendoza, R. Schmidt, R. Bratschitsch, J. Liu, L. Fu, D. Dumcenco, A. Kis, A. Castellanos-Gomez, *J. Phys. D: Appl. Phys.* **2017**, 50, 074002.
- [13] R. Frisenda, E. Navarro-Moratalla, P. Gant, D. P. De Lara, P. Jarillo-Herrero, R. V. Gorbachev, A. Castellanos-Gomez, *Chem. Soc. Rev.* **2018**, 47, 53.
- [14] A. Castellanos-Gomez, M. Buscema, R. Molenaar, V. Singh, L. Janssen, H. S. van der Zant, G. A. Steele, *2D Mater.* **2014**, 1, 011002.
- [15] C. Reuter, R. Frisenda, D. Y. Lin, T. S. Ko, D. Perez de Lara, A. Castellanos-Gomez, *Small Methods* **2017**, 1, 1700119.
- [16] A. J. Molina-Mendoza, M. Barawi, R. Biele, E. Flores, J. R. Ares, C. Sánchez, G. Rubio-Bollinger, N. Agrait, R. D'Agosta, I. J. Ferrer, A. Castellanos-Gomez, *Adv. Electron. Mater.* **2015**, 1, 1500126.
- [17] a) D. Tan, W. Zhang, X. Wang, S. Koirala, Y. Miyauchi, K. Matsuda, *Nanoscale* **2017**, 9, 12425; b) L. Ye, P. Wang, W. Luo, F. Gong, L. Liao, T. Liu, L. Tong, J. Zang, J. Xu, W. Hu, *Nano Energy* **2017**, 37, 53.
- [18] a) J. Miao, B. Song, Z. Xu, L. Cai, S. Zhang, L. Dong, C. Wang, *Small* **2018**, 14, 1702082; b) G. Li, W. Wang, Y. Wang, W. Yang, L. Liu, *Opt. Express* **2016**, 24, 400.
- [19] a) J. Wang, M. S. Gudiksen, X. Duan, Y. Cui, C. M. Lieber, *Science* **2001**, 293, 1455; b) M. Freitag, Y. Martin, J. Misewich, R. Martel, P. Avouris, *Nano Lett.* **2003**, 3, 1067.